AJNR

Deep Learning–Based Super-Resolution Reconstruction on Undersampled Brain Diffusion-Weighted MRI for Infarction Stroke: A Comparison to Conventional Iterative Reconstruction

Shuo Zhang, Meimeng Zhong, Hanxu Shenliu, Nan Wang, Shuai Hu, Xulun Lu, Liangjie Lin, Haonan Zhang, Yan Zhao, Chao Yang, Hongbo Feng and Qingwei Song

AJNR Am J Neuroradiol published online 20 December 2024
http://www.ajnr.org/content/early/2024/12/20/ajnr.A8482

Published December 20, 2024 as 10.3174/ajnr.A8482

Deep Learning–Based Super-Resolution Reconstruction on Undersampled Brain Diffusion-Weighted MRI for Infarction Stroke: A Comparison to Conventional Iterative Reconstruction

Shuo Zhang, Meimeng Zhong, Hanxu Shenliu, Nan Wang, Shuai Hu, Xulun Lu, Liangjie Lin, Haonan Zhang, Yan Zhao, Chao Yang, Hongbo Feng, and Qingwei Song

ABSTRACT

BACKGROUND AND PURPOSE: DWI is crucial for detecting infarction stroke. However, its spatial resolution is often limited, hindering accurate lesion visualization. Our aim was to evaluate the image quality and diagnostic confidence of deep learning (DL)-based super-resolution reconstruction for brain DWI of infarction stroke.

MATERIALS AND METHODS: This retrospective study enrolled 114 consecutive participants who underwent brain DWI. The DWI images were reconstructed with 2 schemes: 1) DL-based super-resolution reconstruction (DWI_{DL}); and 2) conventional compressed sensing reconstruction (DWI_{CS}). Qualitative image analysis included overall image quality, lesion conspicuity, and diagnostic confidence in infarction stroke of different lesion sizes. Quantitative image quality assessments were performed by measurements of SNR, contrast-to-noise ratio (CNR), ADC, and edge rise distance. Group comparisons were conducted by using a paired *t* test for normally distributed data and the Wilcoxon test for non-normally distributed data. The overall agreement between readers for qualitative ratings was assessed by using the Cohen κ coefficient. A *P* value less than .05 was considered statistically significant.

RESULTS: A total of 114 DWI examinations constituted the study cohort. For the qualitative assessment, overall image quality, lesion conspicuity, and diagnostic confidence in infarction stroke lesions (lesion size <1.5 cm) improved by DWI_{DL} compared with DWI_{CS} (all $P < .001$). For the quantitative analysis, edge rise distance of DWI_{DL} was reduced compared with that of DWI_{CS} ($P < .001$), and no significant difference in SNR, CNR, and ADC values (all $P > .05$).

CONCLUSIONS: Compared with the conventional compressed sensing reconstruction, the DL-based super-resolution reconstruction demonstrated superior image quality and was feasible for achieving higher diagnostic confidence in infarction stroke.

ABBREVIATIONS: CNN = convolutional neural network; CNR = contrast-to-noise ratio; CS = compressed sensing; DL = deep learning;; DWI_{CS} = conventional compressed sensing reconstruction; DWI_{DL} = DL-based super-resolution reconstruction; ERD = edge rise distance; IQR = interquartile range

DWI, a powerful MRI tool, is indispensable for the early detection and characterization of ischemic strokes.[1] Ischemic strokes, resulting from the occlusion of intracranial blood vessels, lead to a decreased blood supply to specific brain regions. This deprivation of oxygen and nutrients, along with impaired waste elimination, triggers the cessation of normal neuronal function, potentially progressing to necrosis and permanent infarction if left untreated.[2,3] The unique capability of DWI to detect the diffusion movement of water molecules within tissue provides invaluable insights into the pathophysiologic states of the brain, offering signals that are not captured by conventional MRI sequences. Specifically, DWI can reveal the extent of water molecule diffusion, which is altered in the presence of ischemic injury, enabling the earlier detection of signal abnormalities in infarct lesions and enhancing the diagnostic rate for hyperacute cerebral infarction in clinical settings.[4-6] Conventional DWI, which relies on EPI acquisition, often exhibits limited spatial resolution compared with other routine neuroimaging modalities, which is due to the heightened sensitivity of DWI to B0 inhomogeneities and the stringent requirements for magnetic field gradient hardware. These limit the ability of DWI to visualize and analyze brain tissues with precision, particularly in the context of diseases that require high-quality imaging. To address these challenges, various reconstruction techniques have been developed to enhance the image quality of DWI, including parallel imaging

Received April 16, 2024; accepted after revision July 26.

From the Departments of Nuclear Medicine (S.Z., H.F.), and Radiology (M.Z., N.W., S.H., X.L., H.Z., C.Y., Q.S.), The First Affiliated Hospital of Dalian Medical University, Dalian, China; Department of Radiology (H.S.), Shengjing Hospital of China Medical University, Shenyang, China; Support (L.L.), Philips Healthcare, Beijing, China; and Department of Information Center (Y.Z.), The First Affiliated Hospital of Dalian Medical University, Liaoning, China.

Shuo Zhang and Meimeng Zhong are co-first authors.

Hongbo Feng and Qingwei Song are co-corresponding authors.

Please address correspondence to Qingwei Song, Department of Radiology, The First Affiliated Hospital of Dalian Medical University, Dalian, 116011, China; e-mail: songqw1964@163.com

http://dx.doi.org/10.3174/ajnr.A8482

SUMMARY

PREVIOUS LITERATURE: Deep learning reconstruction has been effective in enhancing image quality in multiple MRI sequences, but its application in super-resolution reconstruction for brain DWI in diagnosing infarction stroke is uncertain.

KEY FINDINGS: The study used a DL-based super-resolution reconstruction technique for brain DWI, which improved overall image quality and diagnostic confidence for infarction stroke compared with traditional DWI reconstructed by compressed sensing.

KNOWLEDGE ADVANCEMENT: Super-resolution reconstruction for brain DWI by using the DL-based method has potential value for early detection of microinfarct lesions and thus provides accurate imaging information for clinical thrombolytic therapy.

and compressed sensing (CS), which can help reduce the geometric distortion and increase the SNRs for DWI.[7,8]

More recently, the deep learning (DL)-based reconstruction algorithms have also been introduced for improved image quality of MRI through denoising and/or super-resolution reconstruction.[9-11] DL-based super-resolution reconstruction has shown promise in various applications,[12-14] including DWI of the prostate[15] and whole spine.[16] However, the application of these techniques to brain DWI remains relatively underexplored, presenting a significant opportunity for advancement in neurologic diagnostics.

The primary objective of this study is to evaluate performance of the DL-based super-resolution reconstruction on randomly undersampled brain DWI data. Specifically, this study aims to assess the efficacy of DL-based super-resolution reconstruction in improving image quality and diagnosis confidence for infarction stroke compared with conventional reconstruction.

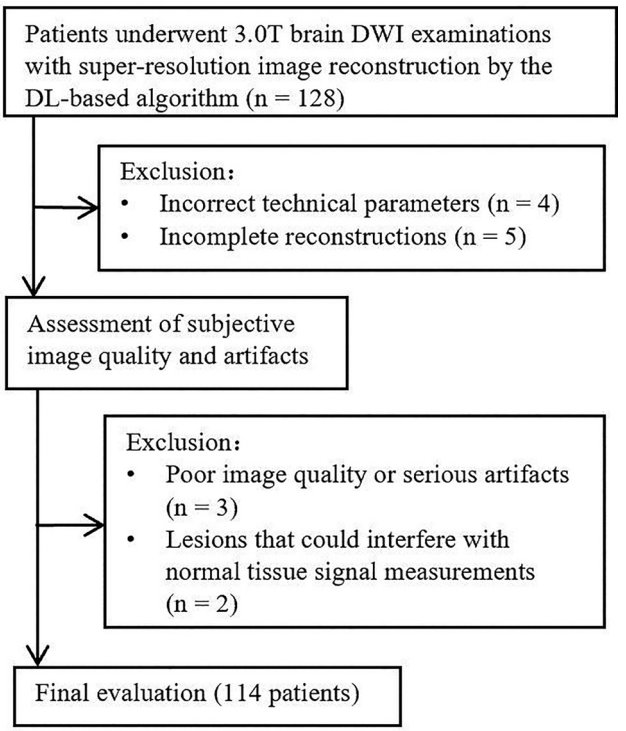

FIG 1. Study flow diagram.

MATERIALS AND METHODS

Study Participants

This retrospective study obtained approval from the institutional review board of The First Affiliated Hospital of Dalian Medical University (Approval No. PJ-KS-KY-2023–261). The study enrolled consecutive patients who underwent brain MRI for screening of stroke from September to December 2023. Exclusion criteria included incorrect technical parameters, incomplete reconstructions, poor image quality, and lesions that could potentially interfere with normal tissue signal measurements (Fig 1).

Brain MRI

Brain MRI was conducted at a 3T scanner (Ingenia CX, Philips Healthcare) by using a 32-channel head coil. MRI scans included T2WI, T1WI, FLAIR, and DWI. DWI was acquired based on the single-shot EPI sequence with 2 b-values (0 and 1000 s/mm^2) with a randomly undersampling factor of 2 in the phase-encoding direction and a 24-second acquisition duration.

All DWI data underwent reconstruction by using 2 methods: 1) DL-based super-resolution reconstruction (DWI_{DL}) and 2) conventional compressed sensing reconstruction (DWI_{CS}).

CS utilizes the algorithm presented in Equation 1, which is primarily based on the method outlined by Lustig and Pauley[17]:

$$p = \min\left(\sum_{i=1}^{\#coils} \| m_{d,i} - ES_{d,i}\, p \|_2^2 + \lambda_1 \| R^{-1\backslash 2}\, p \|_2^2 + \lambda_2 \| \Psi p \|_1\right)$$

Here, p represents the image being reconstructed; $m_{d,i}$ is the measured data for each coil element following noise decorrelation; E is the undersampling Fourier operator determined by the sampling scheme; $S_{d,i}$ denotes the coil sensitivity for each element after noise decorrelation, obtained via the SENSE reference scan; λ_1 is a regularization parameter that mediates between data fidelity and prior image information; R involves the coarse-resolution data from the integrated body coil, derived from the SENSE reference scan and used to guide the regularization; λ_2 is a regularization factor controlling the trade-off between sparsity and data consistency in the iterative process; and Ψ denotes the sparsity transform into the wavelet domain.

The DL super-resolution reconstruction algorithm,[18,19] provided by Philips Healthcare, was utilized, with only nonindustry-affiliated authors having complete access to and control over the data used in this study. This DL-driven reconstruction approach

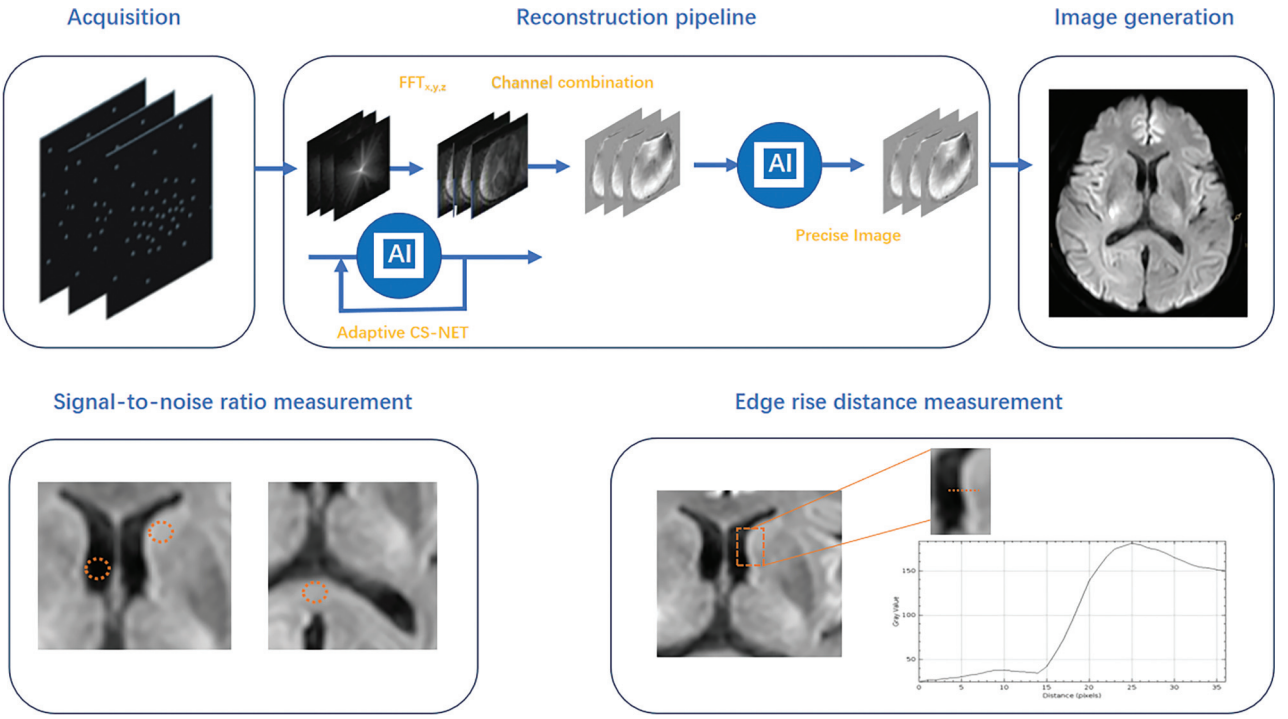

FIG 2. Reconstruction pipeline and quantitative evaluation method diagram.

leverages 2 convolutional neural networks (CNNs), starting with Adaptive-CS-Net,[20] which is capable of reconstructing images from nonuniformly randomly subsampled MRI data. This CNN is applied before coil combination to remove noise from the images, thus ensuring the preservation of high image quality from the expedited acquisition process. An extra network, termed Precise-Image-Net, has been previously evaluated on prostate DWI and T2WI[19,21] as a replacement for the traditional zero-filling strategy, aiming to increase the image matrix size and thereby enhance image sharpness. Precise-Image-Net is an artificial intelligence model designed to remove ringing artifacts and is categorized as a Super Resolution network. It is trained on 6 million pairs of images, comprising low- and high-resolution data with *k*-space crops to induce ringing. Data consistency checks are implemented to ensure that the resulting *k*-space aligns with the measured *k*-space data. The full reconstruction pipeline utilizing Precise-Image-Net generates images with improved SNR and sharpness, higher matrix size, and reduced ringing artifacts, making it applicable to all 2D Cartesian acquisitions.[22,23] Fig 2 provides a graphic representation of the MRI chain, offering a detailed perspective on the reconstruction pipeline. DWI_{DL} reconstruction procedures last approximately 42 seconds, by using the NVIDIA RTX5000 GPU, while the image reconstruction procedure will not impact the data acquisition of subsequent MRI sequences.

Qualitative Image Analysis

Qualitative analysis was independently conducted by 2 experienced radiologists (N.W. and S.H., with 5 and 6 years of expertise in evaluating brain MRI, respectively). The readers were blinded to reconstruction methods, and no washout period was implemented between qualitative evaluations. Categories assessed for both DWI_{CS} and DWI_{DL} included artifacts (motion, partial volume, and susceptibility artifacts), image sharpness (comprising white matter, gray matter, and CSF spaces), and overall image quality (providing a general impression of the image). Additionally, readers reported on lesion conspicuity (identifying suspicious lesions) and lesion measurements (accurate delineation of lesion boundaries within the brain). A 5-point Likert scale ranging from no confidence (1 point) to very high confidence (5 points) was used.

Quantitative Image Analysis

Quantitative analysis involved the calculation of the apparent SNR (signal intensity in WM or GM divided by the signal standard deviation of CSF) and the apparent contrast-to-noise ratio (CNR, [signal intensity of WM or GM minus signal intensity of CSF] divided by the standard deviation of CSF). The analysis focused on the slice level of the corpus callosum and the caudate nucleus. A circular ROI (20 mm^2) was placed within homogeneous and artifact-free zones of these 2 cerebral structures on DWI (b-value of 1000 s/mm^2) with and without DL-based super-resolution reconstruction. The same ROIs were utilized to determine the ADC values of the corpus callosum and caudate nucleus on the ADC map.

Image sharpness was assessed through the determination of the edge rise distance (ERD), defined as the distance between points corresponding to 10% and 90% of the maximum intensity value.[24-26] Smaller ERD values were indicative of superior sharpness. ERD measurements on the DWI (b-value of 1000 s/mm^2) at the interface between brain parenchyma and CSF were conducted by a technician (M.Z.), utilizing the ImageJ software (https://imagej.net/ij/). The particle analysis tool, specifically the Plot

Profile function, was used to generate profile curves. Fig 2 demonstrates ROI examples and the measurement methods.

Diagnostic Confidence in Infarction Stroke Assessment

Lesions of various sizes were included to evaluate the diagnostic confidence of infarction stroke assessment. The radiologists were blinded to both the participant and the DWI method used. For each lesion, the radiologists were provided with routine MRI, and DWI with a b-value of 1000 s/mm^2 and ADC maps from both DWI_{CS} and DWI_{DL}, presented axially in a random order. The readers measured the maximum diameter of infarction lesions on 2D cross-sections of DWI ($b = 1000$ seconds/mm^2) and calculated lesion-average ADC by using a freehand 2D ROI on a representative section for lesion size categorization. Readers reported their diagnostic confidence in infarction assessment. A Likert scale was used to assess each category.

Statistical Analysis

The statistical analysis was conducted by using SPSS (Version 27; IBM). Continuous variables representing quantitative measurements are presented as means ± standard deviation, while discrete variables for qualitative assessment are reported as medians with interquartile range (IQR). Group comparisons between DWI_{DL} and DWI_{CS} were conducted by using a paired *t* test for normally distributed data and the Wilcoxon test for non-normally distributed data.

The overall agreement between readers for qualitative ratings was assessed by using the Cohen κ coefficient (<0.5 = poor; 0.5 to <0.75 = moderate; 0.75 to <0.9 = good; ≥0.9 = excellent). Intrareader reproducibility for quantitative analysis of SNR, CNR, ADC, and ERD was evaluated in a randomly chosen subset of 10 participants, utilizing the 2-way mixed absolute agreement intraclass correlation coefficient (poor: <0.5; moderate: 0.5 to <0.75; good: 0.75 to <0.9; excellent: ≥0.9). Descriptive statistics and visual diagrams were used to illustrate results for direct comparisons. A *P* value less than .05 was considered statistically significant.

Table 1: Clinical characteristics of enrolled participants[a]

Variable	Value
No. of participants	114
Age (y)[b]	59 ± 17
Sex	
Female	55
Male	59
Patients with brain ischemic stroke	
Acute	22 (19.3)
Chronic	39 (34.2)
Healthy subjects	53 (46.4)

[a] Unless otherwise specified, data are numbers of participants, with percentages in parentheses.
[b] Data are means ± standard deviations.

RESULTS

Clinical Characteristics of Participants

After excluding 4 participants with incorrect imaging parameters, 5 participants with incomplete reconstructed DWI, 3 participants with poor image quality, and 2 participants with lesions that could potentially interfere with normal tissue signal measurements, a total of 114 participants, with a mean age of 59 ± 17 years (ranging from 20 to 94 years), were finally included in this study. Detailed participant characteristics are provided in Table 1.

Comparison of Qualitative Image Evaluations

On the 5-point Likert scale for image quality, when compared with DWI_{CS}, DWI_{DL} achieved higher reader scores for the qualitative assessment of image sharpness (reader-averaged median score, 4 [IQR, 4–4] versus 3 [IQR, 3–3], $P < .001$), lesion conspicuity (reader-averaged median score, 4 [IQR, 3–4] versus 3 [IQR, 3–4], $P < .001$), and lesion size measurements (reader-averaged median score, 4 [IQR, 4–4] versus 3 [IQR, 3–3], $P < .001$), as shown in Table 2. For the assessment of image artifacts and overall image quality, DWI_{DL} images received an average of 0.3 and 0.2 points higher than DWI_{CS} (both $P < .001$).

Cohen κ demonstrated moderate to good agreement across all qualitative categories assessed, ranging from 0.59 to 0.88. Average qualitative scores of the 2 readers and 95% CI for each category are reported in Table 2, respectively. Representative participant images are displayed in Fig 3 and 4.

Comparison of Quantitative Image Evaluations

The SNR of DWI_{DL} was 24.1 ± 10.3 for WM and 27 ± 12.3 for GM, showing no significant difference to those of DWI_{CS} (25.1 ± 10 for WM and 27.7 ± 11.5 for GM; $P = .138$ and 0.264, respectively). Similarly, the CNR of DWI_{DL} (17.6 ± 8.6 for WM and 20.4 ± 10.5 for GM) did not exhibit a significant difference from those of DWI_{CS} (18.5 ± 8.4 for WM and 21.2 ± 9.9 for GM; $P = .066$ and 0.174, respectively). The mean ADC for WM was 0.8 ± 0.04 mm^2/s and for GM was 0.72 ± 0.5 mm^2/s for DWI_{DL} demonstrating no significant difference compared with DWI_{CS} (0.8 ± 0.04 mm^2/s for WM and 0.73 ± 0.5 mm^2/s for GM; $P = .136$ and 0.67, respectively). The mean ERD was lower for DWI_{DL} (11.09 ± 5.10 px) compared with DWI_{CS} (13.17 ± 5.50 px; $P < .001$). Fig 5 show comparisons of all of these quantitative evaluations.

The intraclass correlation coefficient for intrareader reproducibility of quantitative measurements was good for ERD (0.77 [95% CI: 0.43–0.91]), SNR (0.82 [95% CI: 0.66–0.91]), and CNR (0.85 [95% CI: 0.72–0.92]), and excellent for ADC value (0.987 [95% CI: 0.98–0.99]).

Table 2: Qualitative image evaluation ratings based on the average score assigned by 2 readers[a]

Category	DWI_{CS}	DWI_{DL}	κ-value[b]	*P*
Image artifacts	3 (2–3)	3 (3–3)	0.82 (0.71–0.91)	<.001
Image sharpness	3 (3–3)	4 (4–4)	0.88 (0.81–0.92)	<.001
Overall image quality	4 (4–4)	4 (4–4)	0.59 (0.41–0.75)	<.001
Lesion conspicuity	3 (3–4)	4 (3–4)	0.76 (0.55–0.91)	<.001
Lesion size measurements	3 (3–3)	4 (4–4)	0.85 (0.7–0.96)	<.001

[a] Unless otherwise specified, data are medians, with IQRs in parentheses. A 5-point Likert scale was used for each category (1 = nondiagnostic to 5 = excellent).
[b] Data in parentheses are 95% CIs.

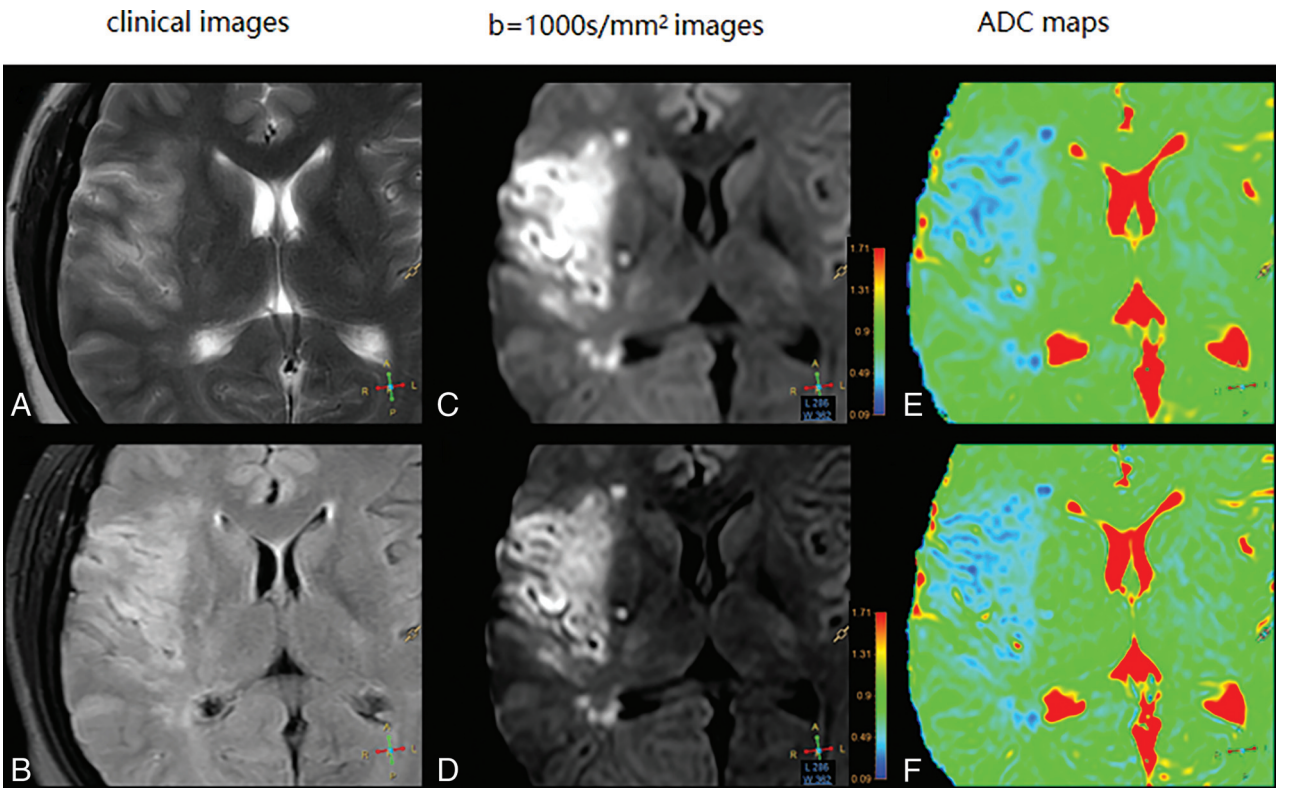

FIG 3. (*A*) T2WI and (*B*) FLAIR image for assessment of an acute cerebral infarction in a 35-year-old female patient. (*C–D*) DWIs ($b = 1000$ s/mm^2) for DWI_{CS} image and DWI_{DL} image, respectively; (*E–F*) ADC maps for DWI_{CS} and DWI_{DL}, respectively.

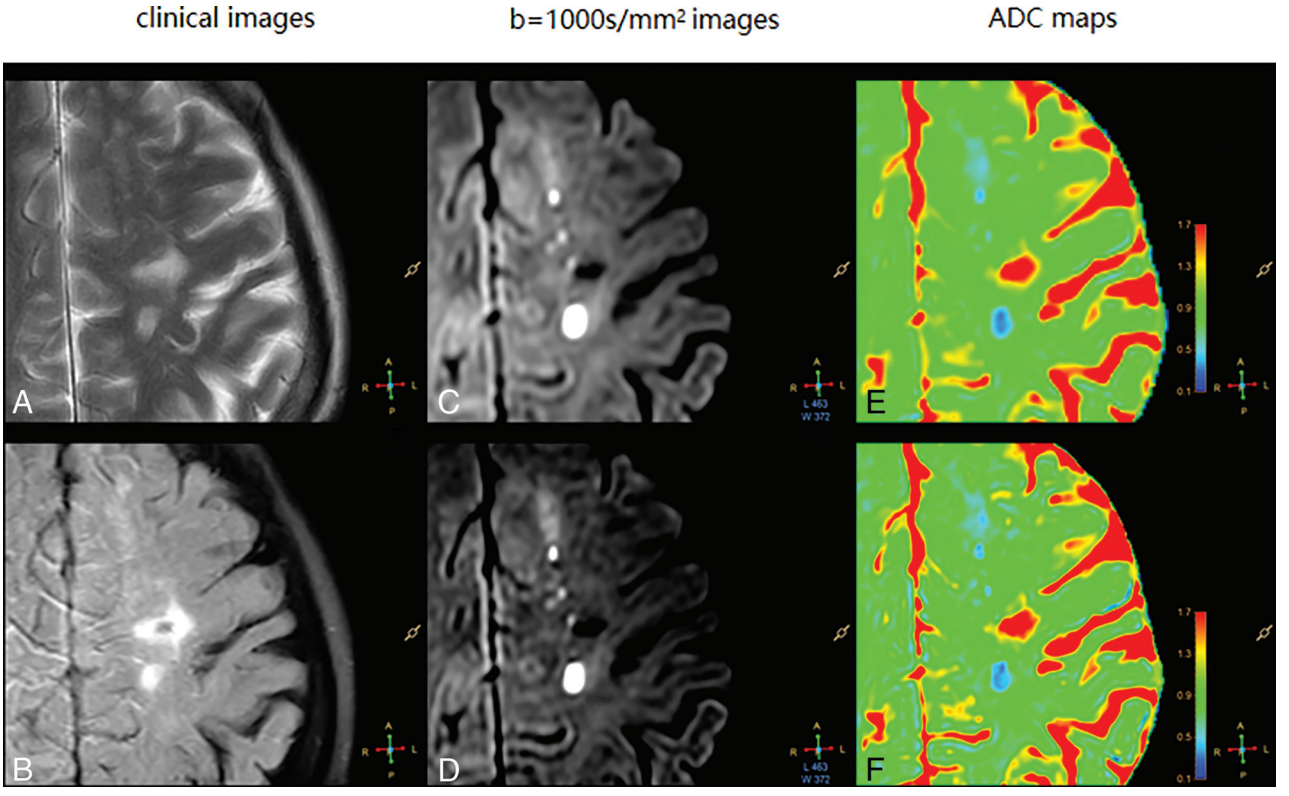

FIG 4. (*A*) T2WI and (*B*) FLAIR image for assessment of an acute cerebral infarction in a 70-year-old female patient. (*C–D*) DWI ($b = 1000$s/mm^2) for DWI_{CS} image and DWI_{DL} image, respectively; (*E–F*) ADC maps for DWI_{CS} and DWI_{DL}, respectively.

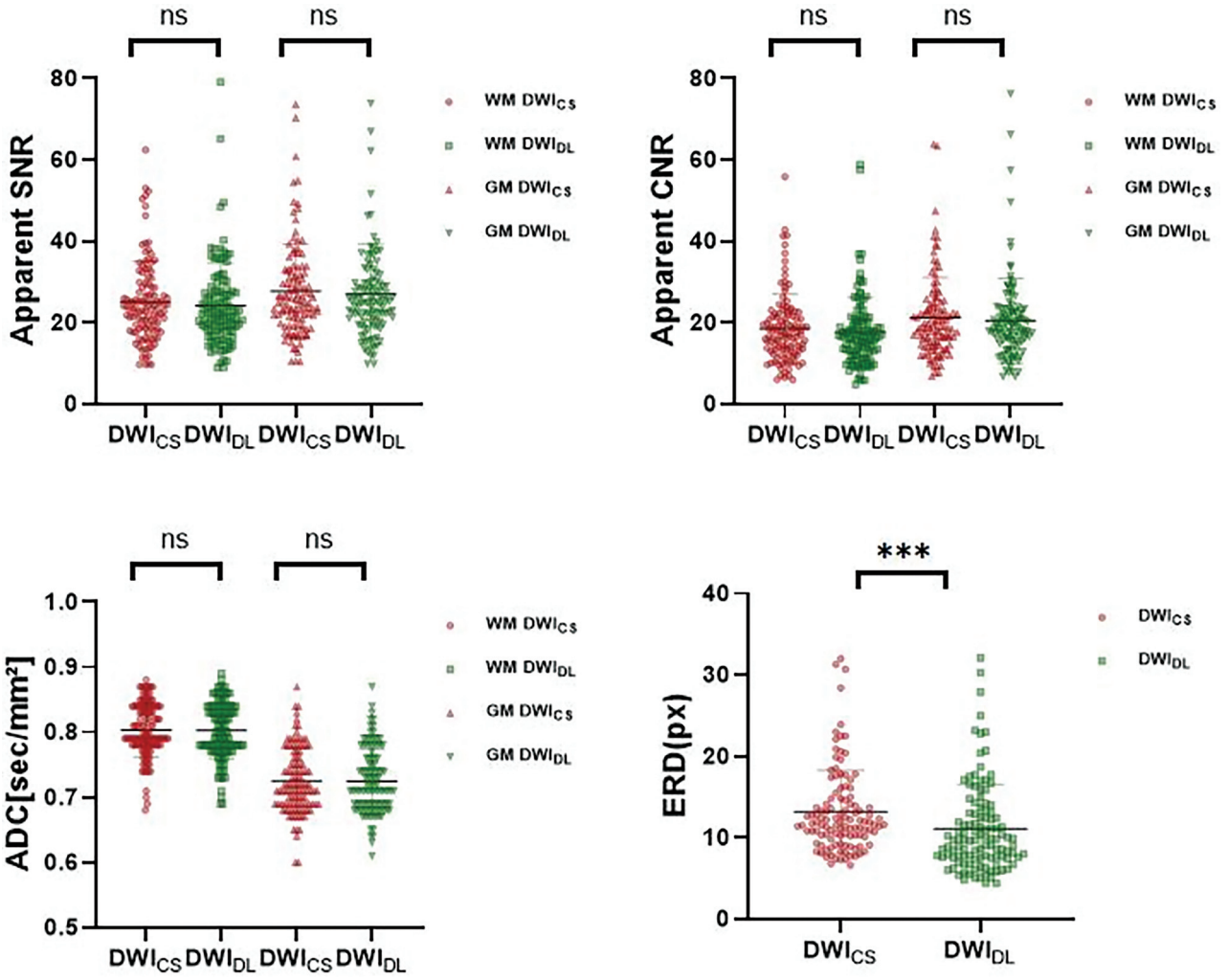

FIG 5. A comparison of apparent SNR, CNR, ADC, and ERD between DWI_{CS} and DWI_{DL}. No significant difference was observed in SNR and CNR between DWI_{DL}; There were no significant difference between DWI_{DL} and DWI_{CS} in the ADC values. The mean ERD of DWI_{DL} was lower than DWI_{CS}. Horizontal dotted lines indicate the mean values. The statistically significant level, ***$P < .001$.

Table 3: Diagnostic confidence of infarction stroke of reader 1 (n=119)[a]

	Diagnostic Confidence Scores		
	DWI_{CS}	DWI_{DL}	*P*
Lesion size <0.5 cm (n=81)	3 (3–3)	4 (4–4)	<.001
Lesion size 0.5–1.5 cm (n=18)	4 (4–4)	5 (4–5)	<.001
Lesion size 1.6–3.0 cm (n=10)	5 (4–5)	5 (5–5)	.05
Lesion size 3.1–5.0 cm (n=5)	5 (4–5)	5 (5–5)	.32
Lesion size >5.0 cm (n=5)	5 (4–5)	5 (5–5)	.32

[a] Unless otherwise specified, data are medians, with IQRs in parentheses. A 5-point Likert scale was used for each category (1 = nondiagnostic to 5 = excellent). Cohen κ for agreement between diagnostic confidence of infarction ratings of the 2 readers was good (lesion size >5.0 cm, 1 [95% CI: 1–1]; lesion size 3.0–5.0 cm, 0.78 [95% CI: 0.28–1]; lesion size 1.5–3.0 cm, 0.69 [95% CI: 0.31–1]; lesion size 0.5–1.5 cm, 0.89 [95% CI: 0.87–1]; lesion size <0.5 cm, 0.86 [95% CI: 0.79–0.94], respectively).

Table 4: Diagnostic confidence of infarction stroke of reader 2 (n=119)[a]

	Diagnostic Confidence Scores		
	DWI_{CS}	DWI_{DL}	*P*
Lesion size <0.5 cm (n=81)	3 (3–3)	4 (4–4)	<.001
Lesion size 0.5–1.5 cm (n=18)	4 (4–4)	5 (4–5)	<.001
Lesion size 1.6–3.0 cm (n=10)	5 (4–5)	5 (5–5)	.03
Lesion size 3.1–5.0 cm (n=5)	5 (4–5)	5 (5–5)	.16
Lesion size >5.0 cm (n=5)	5 (4–5)	5 (5–5)	.32

[a] Unless otherwise specified, data are medians, with IQRs in parentheses. A 5-point Likert scale was used for each category (1 = nondiagnostic to 5 = excellent). Cohen κ for agreement between diagnostic confidence of infarction ratings of the 2 readers was good (lesion size >5.0 cm, 1 [95% CI: 1–1]; lesion size 3.0–5.0 cm, 0.78 [95% CI: 0.28–1]; lesion size 1.5–3.0 cm, 0.69 [95% CI: 0.31–1]; lesion size 0.5–1.5 cm, 0.89 [95% CI: 0.87–1]; lesion size <0.5 cm, 0.86 [95% CI: 0.79–0.94], respectively).

Comparison of Diagnostic Confidence of Infarction Stroke

For the diagnostic confidence of infarction stroke assessment, when compared with DWI_{CS}, DWI_{DL} achieved an averaged reader score of 4 or higher, for lesion sizes <0.5 cm and 0.5–1.5 cm (reader-averaged median score, 4 [IQR, 4–4] versus 3 [IQR, 3–3], 5 [IQR, 4–5] versus 4 [IQR, 4–4], respectively; both $P < .001$). For lesion sizes 1.6–3.0 cm, the average score of reader 2 differed between DWI_{DL} and DWI_{CS} (reader-averaged median score, 5 [IQR, 5–5] versus 5 [IQR, 4–5]; $P = .03$), while there is no difference in the average score of reader 1 between DWI_{DL} and DWI_{CS} (reader-averaged median score, 5 [IQR, 5–5] versus 5 [IQR, 4–5]; $P = .05$). There was no significant difference between DWI_{DL} and DWI_{CS} in the 2

reader-averaged diagnostic confidence of infarction stroke scores, 3.1–5.0 cm and >5.0 cm (reader-averaged median score 5 [IQR, 5–5] versus 5 [IQR, 4–5] for all, $P > .05$ for all) (Table 3 and 4).

DISCUSSION

In this study, a recently introduced DL super-resolution reconstruction technique was used for in-brain DWI, and both qualitative and quantitative comparisons were made with traditional DWI reconstructed by compressed sensing. The secondary objective aimed to assess the diagnostic performance of brain DWI reconstructed with DL for infarction stroke. Results indicated that DL reconstruction improved overall image quality and diagnostic confidence of infarction stroke (lesion size <0.5 cm and 0.5–1.5 cm) with DWI_{DL} in comparison with DWI_{CS} (all $P < .001$).

Traditional MRI reconstruction usually uses complicated mathematical methods and involves complex processes, such as the wavelet transformation for denoising in compressed sensing reconstruction.[27-29] However, new methods are emerging to streamline MRI reconstruction protocols. For example, a recent study suggested that combining random undersampling with DL denoising (Adaptive-CS-Net) can enhance the image quality of MRI compared with using compressed sensing reconstruction.[30] Our study reveals that the addition of an extra neural network[18,19] to enhance image resolution further contributes to improved image quality. This improvement is demonstrated both qualitatively, through image sharpness, and quantitatively, as evidenced by the ERD.

In contrast to other acceleration techniques that may compromise image quality, such as partial Fourier acquisition and parallel imaging,[30,31] the super-resolution network used in our study improved lesion observation without compromising apparent SNR and apparent CNR. Specifically, in lesion conspicuity scoring, DL reconstruction enhanced lesion conspicuity compared with CS reconstruction DWI. The SNR, CNR, and ADC values of DWI_{DL} showed no significant differences compared with those of DWI_{CS}. Notably, DWI_{DL} increased confidence in lesion measurements compared with traditional DWI.

Super-resolution reconstruction for brain DWI has significant potential value for diagnosing lesions smaller than 0.5 cm, offering the chance to discover acute cerebral infarction and strive for the best treatment time. At the same time, it can also provide more intuitive and accurate imaging information for clinical thrombolytic therapy. Results of the current study show that, as infarct lesions decrease in size, the difference in diagnostic confidence between DWI_{DL} and DWI_{CS} becomes more pronounced. This score variation may facilitate early detection of microinfarct lesions, potentially averting oversight, especially in subcortical infarcts that are prone to being overlooked.

Our study has several limitations. First, our study lacks a standard imaging method to validate the diffusion-restricted lesions detected by our DL reconstruction approach. Second, expert readers were employed for subjective image quality assessments, and despite variations in the interpretations of the 5-point Likert scale, the consistency of differences between various imaging methods was maintained. For quantitative evaluations, manual measurements of ROIs may introduce errors, leading to biased results. Third, our study exclusively focused on DL super-resolution reconstruction of DWI, primarily associated with acute ischemic stroke assessment. However, in most chronic cases, FLAIR imaging is equally important.[32] Because the fundamental principles of the DL reconstruction method are not restricted to the DWI sequence, further evaluation is necessary for its application to different weighted sequences. Fourth, a more diverse study sample is needed to evaluate the detection rate thoroughly. Despite these limitations, it is noteworthy that our retrospective analysis of all patients with strokes showed no instances of missed or fabricated lesions in the DL-reconstructed images compared with conventional compressed sensing images, and instead, they notably improved the visibility of lesions, particularly smaller ones. Future studies should address these limitations by broadening the study's scope to encompass other imaging sequences, and enrolling a more diverse patient population. Additionally, it is crucial to use follow-up imaging or clinical correlation to validate the detected lesions.

CONCLUSIONS

We used a newly developed DL-reconstruction method to enhance image resolution and compared it with traditional compressed sensing reconstruction for brain DWI. Due to the improved image resolution, this method may assist in early detection of small infarcts, allowing for timely intervention in such patients. However, the exact impact of this technology on the accuracy of head DWI requires further assessment. Additionally, the impact of this technique on DWI in different anatomic regions remains unclear and warrants in-depth investigation.

Disclosure forms provided by the authors are available with the full text and PDF of this article at www.ajnr.org.

REFERENCES

1. Gaddamanugu S, Shafaat O, Sotoudeh H, et al. **Clinical applications of diffusion-weighted sequence in brain imaging: beyond stroke.** *Neuroradiology* 2022;64:15–30 CrossRef Medline
2. Maguida G, Shuaib A. **Collateral circulation in ischemic stroke: an updated review.** *J Stroke* 2023;25:179–98 CrossRef Medline
3. Popiela T J, Krzyściak W, Pilato F, et al. **The assessment of endovascular therapies in ischemic stroke: management, problems and future approaches.** *J Clin Med* 2022;11:1864 CrossRef
4. Doubal FN, Dennis MS, Wardlaw JM. **Characteristics of patients with minor ischaemic strokes and negative MRI: a cross-sectional study.** *J Neurol Neurosurg Psychiatry* 2011;82:540–42 CrossRef Medline
5. Kawano H, Hirano T, Nakajima M, et al. **Diffusion-weighted magnetic resonance imaging may underestimate acute ischemic lesions: cautions on neglecting a computed tomography-diffusion-weighted imaging discrepancy.** *Stroke* 2013;44:1056–61 CrossRef Medline
6. Sylaja PN, Coutts SB, Krol A, et al; VISION Study Group. **When to expect negative diffusion-weighted images in stroke and transient ischemic attack.** *Stroke* 2008;39:1898–1900 CrossRef Medline
7. Tamada T, Ueda Y, Kido A, et al. **Clinical application of single-shot echo-planar diffusion-weighted imaging with compressed SENSE in prostate MRI at 3T: preliminary experience.** *MAGMA* 2022;35:549–56 CrossRef Medline
8. Kaga T, Noda Y, Mori T, et al. **Diffusion-weighted imaging of the abdomen using echo planar imaging with compressed SENSE: feasibility, image quality, and ADC value evaluation.** *Eur J Radiol* 2021;142:109889 CrossRef Medline

9. Kim M, Lee SM, Park C, et al. **Deep learning-enhanced parallel imaging and simultaneous multislice acceleration reconstruction in knee MRI.** *Invest Radiol* 2022;57:826–33 CrossRef Medline
10. Wang Q, Zhao W, Xing X, et al. **Feasibility of AI-assisted compressed sensing protocols in knee MR imaging: a prospective multi-reader study.** *Eur Radiol* 2023;33:8585–96 CrossRef Medline
11. Pezzotti N, Yousefi S, Elmahdy MS, et al. **An adaptive intelligence algorithm for undersampled knee MRI reconstruction.** *IEEE Access* 2020;8:204825–38 CrossRef
12. Yao T, St Clair N, Miller GF, et al. **A deep learning pipeline for assessing ventricular volumes from a cardiac MRI registry of patients with single ventricle physiology.** *Radiology Artif Intell* 2024;6:e230132 Medline
13. Knuth F, Tohidinezhad F, Winter RM, et al. **Quantitative MRI-based radiomics analysis identifies blood flow feature associated to overall survival for rectal cancer patients.** *Sci Rep* 2024;14:258 CrossRef Medline
14. Li Y, Lv X, Chen C, et al. **A deep learning model integrating multisequence MRI to predict EGFR mutation subtype in brain metastases from non-small cell lung cancer.** *Eur Radiology Exp* 2024;8:2 CrossRef Medline
15. Ueda T, Ohno Y, Yamamoto K, et al. **Deep learning reconstruction of diffusion-weighted MRI improves image quality for prostatic imaging.** *Radiology* 2022;303:373–81 CrossRef Medline
16. Kim DK, Lee S-Y, Lee J, et al. **Deep learning-based k-space-to-image reconstruction and super resolution for diffusion-weighted imaging in whole-spine MRI.** *Magn Reson Imaging* 2024;105:82–91 CrossRef Medline
17. Lustig M, Pauly JM. **SPIRiT: iterative self-consistent parallel imaging reconstruction from arbitrary k-space.** *Magn Reson Med* 2010;64:457–71 CrossRef Medline
18. Chaudhari AS, Fang Z, Kogan F, et al. **Super-resolution musculoskeletal MRI using deep learning.** *Magn Reson Med* 2018;80:2139–54 CrossRef Medline
19. Bischoff LM, Peeters JM, Weinhold L, et al. **Deep learning super-resolution reconstruction for fast and motion-robust T2-weighted prostate MRI.** *Radiology* 2023;308:e230427 CrossRef Medline
20. Pezzotti N, de Weerdt E, Yousefi S, et al. **Adaptive-CS-Net: FastMRI with Adaptive Intelligence.** *arXiv e-prints* 2019 arXiv:1912.12259
21. Jurka M, Macova I, Wagnerova M, et al. **Deep-learning-based reconstruction of T2-weighted magnetic resonance imaging of the prostate accelerated by compressed sensing provides improved image quality at half the acquisition time.** *Quant Imaging Med Surg* 2024;14:3534–43 CrossRef Medline
22. Dong C, Loy CC, He K, et al. **Image super-resolution using deep convolutional networks.** *IEEE Trans Pattern Anal Mach Intell* 2016;38:295–307 CrossRef Medline
23. Li Y, Sixou B, Peyrin F. **A review of the deep learning methods for medical images super resolution problems.** *IRBM* 2020;42:120–33 CrossRef
24. Yeoh H, Hong SH, Ahn C, et al. **Deep learning algorithm for simultaneous noise reduction and edge sharpening in low-dose CT images: a pilot study using lumbar spine CT.** *Korean J Radiol* 2021; 22:1850–57 CrossRef Medline
25. Tatsugami F, Higaki T, Nakamura Y, et al. **Deep learning-based image restoration algorithm for coronary CT angiography.** *Eur Radiol* 2019;29:5322–29 CrossRef Medline
26. Tatsugami F, Higaki T, Sakane H, et al. **Coronary artery stent evaluation with model-based iterative reconstruction at coronary CT angiography.** *Acad Radiol* 2017;24:975–81 CrossRef Medline
27. Jia H, Yin Q, Lu M. **Blind-noise image denoising with block-matching domain transformation filtering and improved guided filtering.** *Sci Rep* 2022;12:16195 CrossRef Medline
28. Yang J, Wang C, Xiang J, et al. **Oral CT image processing based on oral CT image filtering algorithm.** *Comput Intell Neurosci* 2022; 2022:6041872 CrossRef Medline
29. Dwork N, O'Connor D, Baron CA, et al. **Utilizing the wavelet transform's structure in compressed sensing**. *Signal Image Video Process* 2021;15:1407–14 CrossRef Medline
30. Fervers P, Zaeske C, Rauen P, et al. **Conventional and deep-learning-based image reconstructions of undersampled K-space data of the lumbar spine using compressed sensing in MRI: a comparative study on 20 subjects.** *Diagnostics (Basel)* 2023;13:418 CrossRef
31. Chen Y, Li J, Qu X, et al. **Partial Fourier transform reconstruction for single-shot MRI with linear frequency-swept excitation.** *Magn Reson Med* 2013;69:1326–36 CrossRef Medline
32. Zhu H, Jiang L, Zhang H, et al. **An automatic machine learning approach for ischemic stroke onset time identification based on DWI and FLAIR imaging.** *Neuroimage Clin* 2021;31:102744 CrossRef Medline